Energy & Environmental Science

PAPER

View Article Online
View Journal

Cite this: DOI: 10.1039/c4ee01377h

Improved lithium–sulfur batteries with a conductive coating on the separator to prevent the accumulation of inactive S-related species at the cathode–separator interface†

Hongbin Yao,[a] Kai Yan,[a] Weiyang Li,[a] Guangyuan Zheng,[b] Desheng Kong,[a] Zhi Wei Seh,[a] Vijay Kris Narasimhan,[a] Zheng Liang[a] and Yi Cui*[ac]

Received 3rd May 2014
Accepted 14th July 2014

DOI: 10.1039/c4ee01377h

www.rsc.org/ees

Lithium–sulfur (Li–S) batteries are highly attractive for future generations of portable electronics and electric vehicles due to their high energy density and potentially low cost. In the past decades, various novel electrodes and electrolytes have been tested to improve Li–S battery performance. However, these designs on electrodes and electrolytes have not fully addressed the problem of low cycling stability of Li–S batteries. Here, we show the role of the separator in the capacity decay of the Li–S battery, namely that it can accommodate a large amount of polysulfides inside which then precipitates as a thick layer of inactive S-related species. Using a thin conductive coating on the separator to prevent the formation of the inactive S-related species layer, we show that the specific capacity and cycling stability of the Li–S battery are both improved significantly compared to the battery with a pristine separator. Combining this separator design with a monodisperse sulfur nanoparticle cathode, we show Li–S batteries with a life of over 500 cycles with an initial specific capacity of 1350 mA h g^{-1} at C/2 and a cycle decay as low as 0.09% per cycle.

Broader context

High energy density rechargeable batteries are highly demanded in energy storage systems for portable electronics, vehicle electrification, and grid-scale stationary storage. Lithium–sulfur (Li–S) batteries are attractive due to their high theoretical energy density (2600 W h kg^{-1}, 2800 W h L^{-1}) and reasonable kinetics. On the S cathode, intermediate polysulfide dissolution coupled with large volume change and low electronic and ionic conductivity of solid S-related species has resulted in poor cycle performance and low practical energy. To address these challenging issues in Li–S batteries, rational designs are desired in the Li–S battery system including the electrode, the electrolyte, and the separator. Here, we show that the separator can accommodate a large amount of polysulfides inside which then precipitates as a thick layer of inactive S-related species on the surface of the cathode. With a novel design of a thin conductive coating on the separator to prevent the formation of the inactive S-related species layer, we demonstrate that the specific capacity and cycling stability of the Li–S battery are both improved significantly compared to the battery with a pristine separator.

Introduction

There is a large demand for high energy density rechargeable batteries for portable electronics, vehicle electrification and grid-scale stationary storage systems.[1,2] To satisfy the advanced energy storage demand, various rechargeable battery systems such as aqueous rechargeable lithium ion batteries,[3] flexible lithium ion batteries,[4] and sodium ion batteries have been developed.[5,6] Among the proposed rechargeable battery systems, Li–S batteries are especially attractive due to their high theoretical energy density (2600 W h kg^{-1}, 2800 W h L^{-1}, respectively) and low cost.[7–10] However, the practical energy density and cycling stability of the Li–S battery are limited by the low electronic and ionic conductivity of solid S-related species, large volume changes, and the dissolution of intermediate polysulfides in the electrolyte.[11–15] During the cycling of Li–S batteries, solid S or Li_2S_x ($x = 1$ or 2) cathodes go through a series of intermediate polysulfide species (Li_2S_x, $x = 8$, 6, 4, and 3) and become solid Li_2S_x ($x = 1$ or 2) or S.[16,17] The higher-order lithium polysulfides (*e.g.*, Li_2S_8 and Li_2S_6) are highly soluble in the electrolyte and would diffuse throughout the whole cell, leading to the shuttle effect and capacity loss of active materials, which are thought to be the main reasons for low Coulombic efficiency and rapid capacity fade in Li–S batteries.[11,18]

[a]Department of Materials Science and Engineering, Stanford University, Stanford, CA 94305, USA. E-mail: yicui@stanford.edu

[b]Department of Chemical Engineering, Stanford University, Stanford, CA 94305, USA

[c]SLAC National Accelerator Laboratory, Stanford Institute for Materials and Energy Sciences, 2575 Sand Hill Road, Menlo Park, CA 94025, USA

† Electronic supplementary information (ESI) available. See DOI: 10.1039/c4ee01377h

To address these challenging issues in Li–S batteries, rational designs are desired in the Li–S battery system including the electrode, the electrolyte, and the separator.[19,20] For the electrode design, nano-porous carbon and conducting polymers have been used to encapsulate sulfur inside in order to improve the conductivities of S-related species and to trap the polysulfides in the cathode.[21–26] These conductive frameworks can improve the utilization of sulfur at the initial cycle, while the fast capacity decay in the subsequent cycles shows that the porous conductive matrix cannot prevent the dissolution of polysulfides. The core/shell sulfur/polymer and yolk–shell sulfur/TiO_2 nanostructures with a pre-designed interior hollow space have also been designed to trap polysulfide and accommodate volume expansion of sulfur.[27,28] Although an excellent cycle life of Li–S battery up to 1000 cycles has been achieved with these core/shell hollow nanostructures, there is still ~20 wt% polysulfide leaking into the electrolyte. Recently, the freestanding conductive bifunctional interlayer design has shown the promise to improve the performance of the Li–S battery.[29,30] However, the thickness (tens of micrometers) and the mass (several milligrams) of these interlayers are rather large, which if not reduced would substantially decrease the specific capacity of the cell.

Many novel electrolytes have been tried in Li–S batteries as well. For example, solid electrolytes including polymer electrolytes[31–33] and glass–ceramic electrolytes[34,35] have been studied in Li–S batteries in order to avoid the dissolution of polysulfides. The low lithium ion conductivity in solid electrolytes and their stability and processability remain to be addressed. The 'solvent-in-salt' design of an electrolyte has been proposed to retard the dissolution of polysulfides in the electrolyte and suppress the formation of Li dendrites during cycling.[36]

Compared with the intensive studies focused on the electrode and the electrolyte, the influence of the separator on the cell performance has rarely been studied in the Li–S batteries. Only recently, a Nafion barrier layer and a graphene layer on the separator have been tried to prevent the migration of polysulfides from the S cathode to the Li metal anode in Li–S batteries.[37–39] The details of the diffusion of polysulfides in the separator and the separator's impact on the performance of Li–S batteries have not been unveiled. We believe that exploring separators for improving Li–S batteries is a worthwhile field of inquiry but that it is only in its infancy.

The separator is a critical component in the lithium ion battery. It is a nanoporous polymer membrane with a porosity of up to 50% for maintaining the diffusion of lithium ions while preventing electrical contact between the cathode and anode.[40] Through the surface modification of the separator, the improved cycling stability and the decreased self-discharge effect have been demonstrated in conventional graphite–lithium metal oxide batteries.[41,42] Unlike conventional graphite–lithium metal oxide lithium ion batteries, the highly soluble polysulfide intermediates in Li–S batteries can diffuse into the separators during the charge/discharge process. The diffusion path and distribution of polysulfides in the separator will provide important information for the rational design of the separator in Li–S batteries. Herein, we show that the nanoporous separator is able to accommodate a large amount of polysulfides inside. When depositing back during charge/discharge, we hypothesize that the polysulfides in the separator would preferentially precipitate close to the top surface of the cathode since this surface is the closest conductive path. To utilize the large amount of polysulfides in the separator, we propose that a high surface area conducting layer should be inserted between the S cathode and the separator for precipitation of S or Li_2S/Li_2S_2. We directly coat a thin, porous conductive layer onto the separator surface *via* a facile slurry coating method. Using this surface modified separator, the specific capacity and cycling stability of Li–S batteries are improved as compared to the batteries with pristine separators. Combining this separator design with uniform sulfur nanoparticles synthesized in our lab, we demonstrate a Li–S battery over 500 cycles with an initial specific capacity of 1350 mA h g^{-1} at C/2 and a decay rate as low as 0.09% per cycle.

Experimental section

Polysulfide diffusion across the separator

A U shape cell separated by a Celgard polyethylene separator (25 μm thick) was used as the electrolyte container for the polysulfide diffusion in the separator. One side of the cell was filled with the blank electrolyte and the other side had the electrolyte with 0.5 M Li_2S_8. The polysulfide diffusion from one side to the other side crossing the separator was recorded optically by using a camera.

Li–S prototype cell for *in situ* Raman

A quartz cell with transparent windows and a rectangle empty space inside was chosen as the cell housing. A carbon fiber paper (Fuel Cell Store Inc) with the size of 5 cm × 0.5 cm × 100 μm and weight of ~25 mg was used as the current collector and electrode. 4 mg of sulfur powder was thermally infused into the carbon fiber paper. The sulfur infused carbon fiber paper, polymer separator, lithium metal, and spring were inserted into the quartz cell. The aluminum foil and copper foil were connected to the carbon fiber paper and lithium metal as electrodes connected to a VMP3 potentiostat (Bio-logic) for cell charge/discharge. The electrolyte (lithium bis(trifluoromethanesulfonyl)imide (1 M) in tetraethylene glycol dimethyl ether, ~50 μL) was injected into the cell. The cell was sealed with a rubber lid. The fabricated cell was put on the stage of a Raman spectrophotometer (Horiba Jobin Yvon Raman equipped with a 532 nm laser) with the transparent window facing the laser for *in situ* characterization.

Separator coating

A slurry method using a doctor blade was employed to coat the separator with a conductive layer. Various conductive materials, namely a mixture of carbon nanomaterials and polyvinylidene fluoride (PDVF) as the binder with a weight ratio of 9 : 1, or a mixture of metal oxides nanoparticles, carbon black (Super P), and PVDF with a weight ratio of 4.5 : 4.5 : 1 was dispersed into *N*-methylpyrrolidinone (NMP, Sigma-Aldrich) forming a slurry.

The obtained slurry was coated on one side of a Celgard PP separator (25 μm thick) with a doctor blade (3 milli-inch). The slurry coated separator was dried in a vacuum oven at 50 °C for 12 hours. Finally, the dried nanoparticle-coated separator was punched into a disk with a diameter of 5/8 inch (1.58 cm) for assembling cells.

Sulfur cathode preparation

The sulfur cathode was prepared by conventional slurry coating. The slurry was prepared by mixing commercial sulfur powder, Super P, and PVDF with desired ratios in an *N*-methylpyrrolidinone (NMP, Sigma-Aldrich) solution overnight. The slurry was spread on the carbon coated aluminum substrate (MTI) by a doctor blade (20 milli-inch) and dried in a vacuum oven at 50 °C for 5 hours. The sulfur mass loading in the cathode is 1.5–2 mg cm^{-2}. The preparation of the polypyrrol coated sulfur NP cathode was reported in our previous work.[43]

Electrochemistry

To evaluate the electrochemical performance of the modified separator, 2023 type coin cells (MTI) were assembled using lithium metal as the counter/reference electrode. The electrolyte was a freshly prepared solution of lithium bis(trifluoromethanesulfonyl)imide (1 M) in 1 : 1 v/v 1,2-dimethoxyethane and 1,3-dioxolane (DOL) containing $LiNO_3$ (1 wt%). 2032-type coin cells were assembled in an argon-filled glove box and galvanostatic cycling of cells was carried out using a 96-channel battery tester (Arbin Instruments). Electrochemical impedance spectroscopy data were obtained with a VMP3 potentiostat (Bio-logic) from 200 KHz to 100 mHz with an AC voltage amplitude of 10 mV at the open-circuit voltage of the cells with the Li metal foil as both auxiliary and reference electrodes.

Characterization

An FEI XL30 Sirion scanning electron microscope (SEM) with an FEG source was used for SEM characterization. The cathodes for SEM characterization were washed with DOL thoroughly in the glove box. The Raman spectra were recorded by using a Horiba Jobin Yvon Raman equipped with a 532 nm laser.

Results and discussion

To study the influence of separator on the distribution of polysulfides in a Li–S battery, the diffusion of the polysulfides across the separator was first investigated based on a simple U-shape diffusion model. As shown in Fig. 1, the U-shape cell was split by the commercial Celgard polyethylene separator (25 μm thick). One side of the cell was filled with the blank electrolyte and the other side had the electrolyte with 0.5 M Li_2S_8. Driven by the concentration gradient, the Li_2S_8 would diffuse from one side to the other side across the separator. But this diffusion process was slowed down by the separator due to its nanoporous structure. Even after 30 minutes diffusion, the color of the blank electrolyte did not change and the color in some area of the separator became yellow, which indicated that the Li_2S_8 had filled the separator. With the diffusion time prolonging to 70 minutes, light yellow color appeared in the blank electrolyte and the whole separator became red, which means that the Li_2S_8 fully filled the pores in the separator. The observation of Li_2S_8 diffusion in the U-shape cell shows that the separator can slow down the polysulfide diffusion and accommodate a large amount of polysulfides inside.

In the practical Li–S battery, the soluble polysulfides are intermediates between the transformation of S and Li_2S. To show this phase change process we used the *in situ* Raman spectroscopy to characterize the sulfur species during the cycling. A prototype Li–S cell for Raman characterization is shown in Fig. S1a,† in which a sandwich structure of carbon paper (infused with sulfur), separator, and lithium metal was assembled. The fabricated cell was put on the stage of a Raman spectrophotometer with a transparent window facing to the laser for *in situ* characterization (Fig. S1b†). As shown in Fig. 2a, the Raman spectra were recorded at five states at 2.4 V (A), 2.1 V (B), 1.7 V (C), 2.4 V (D), and 2.6 V (E) respectively in one discharge/charge cycle. Fig. 2b shows the typical Raman spectra collected from the cathode at different states. At the 2.4 V, three peaks at 152 cm^{-1}, 218 cm^{-1}, and 470 cm^{-1} can be assigned to those of solid sulfur (S_8).[17] The Raman spectrum at 2.1 V can be identified as that of polysulfides (S_x^{2-}, $x = 4$–8).[17,44] When the cell was discharged to 1.7 V, the Raman spectrum shows the existence of Li_2S and Li_2S_2 in the cathode.[44] After charging the cell to 2.4 V, the Li_2S and Li_2S_2 species changed back to polysulfides again. With charging to 2.6 V, the polysulfides further transformed to S_8.[17,44] From these Raman spectra, it can be clearly seen that the polysulfides appeared twice during one discharge/charge cycle.

Due to the high porosity of the separator to accommodate polysulfides as shown in Fig. 1, the amount of the polysulfide in the separator (25 μm, 50% porosity) during Li–S cell cycling can be as high as ~0.2 mg cm^{-2} of sulfur (the detailed calculation is provided in the ESI†), which is about 20% of the total active materials if the sulfur mass loading in the cathode is 1 mg cm^{-2}. Taking into consideration the polysulfides in the separator, the distribution of sulfur species in the Li–S battery during cycling is schematically illustrated in Fig. 2c. Initially, the separator between the Li anode and the S cathode is free of S species. During the discharging process to 2.1 V, the yielded polysulfides (*e.g.*, Li_2S_8 and Li_2S_6) would dissolve into the electrolyte and diffuse into the separator. While discharging the cell to 1.7 V, the polysulfides in the separator tend to precipitate as lithium sulfides on the top surface of the cathode, which is the conducting surface at the shortest diffusion distance. When charging the cell from 1.7 V to 2.6 V, polysulfides diffuse back into the separator and then precipitate as S on the top surface of the cathode. The top surface of the cathode offers only a limited conducting surface area for the deposition of S-related species. Sulfur-related species are electronically insulating so that only a thin layer of materials can be deposited onto the conducting surface. These facts would reduce the utilization of the polysulfides accommodated in the separator. Meanwhile, the continuous layer of S-species on the top of the cathode surface would block the diffusion of polysulfides from the separator to

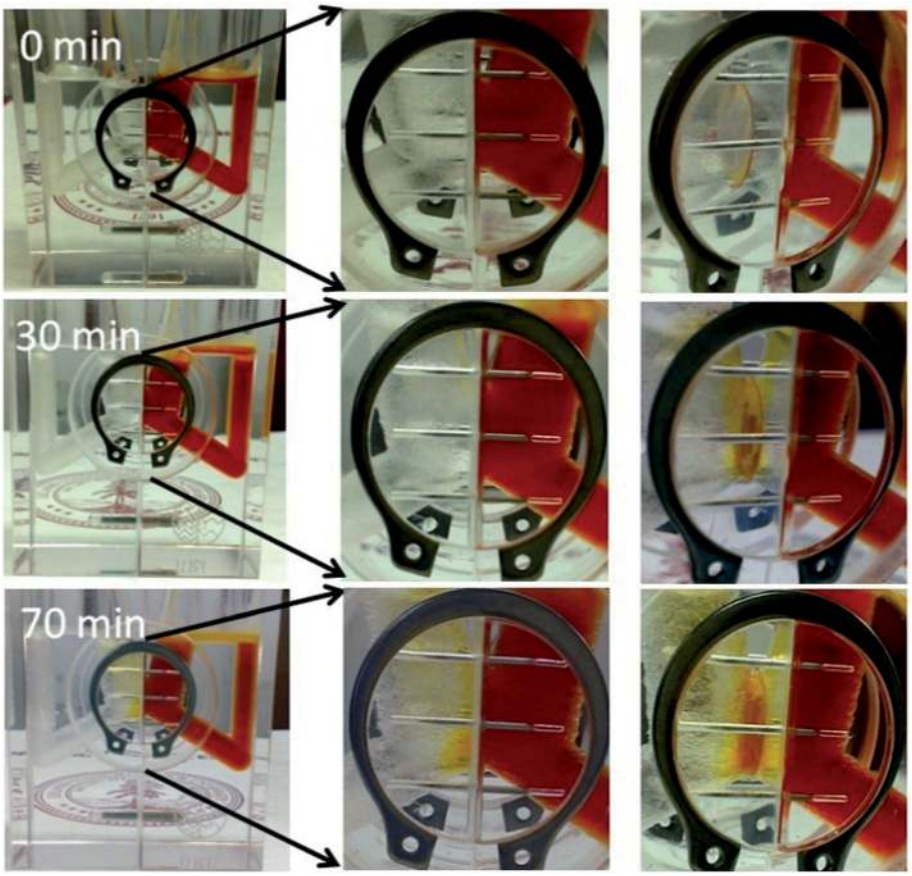

Fig. 1 Photographs recording the polysulfide diffusion process across the separator. In the beginning (0 minute), the polysulfides were totally blocked by the separator from the blank electrolyte. After 30 minutes of diffusion, the Li_2S_8 filled the separator. When the diffusion time prolonged to 70 minutes, the Li_2S_8 fully filled the pores in the separator.

deep inside the cathode. After several diffusion and precipitation cycles, a visible continuous layer of S-species would be formed on the top surface of the cathode.[11,18,45,46] To show this layer, a normal Li–S coin cell was disassembled after 50 cycles with the discharged potential at 1.7 V and the top surface of the cathode was characterized by SEM. The yellow color of the separator (the inset in Fig. 2d) indicates that there were polysulfides in the separator even when the cell was discharged to 1.7 V. The cross sectional SEM image of the cathode (Fig. 2d) shows that the cathode was attached with Al foil and its top surface was covered by a smooth layer. The magnified SEM image (Fig. 2e) further shows that the layer covering on the top surface of the cathode is very dense with a thickness of ~500 nm. The top surface SEM image (Fig. 2f) also indicates that the solid sulfur species layer formed on the top surface of the cathode is very smooth and dense. This solid sulfur species layer surface was further characterized by Raman spectroscopy and compared to the surfaces of a fresh sulfur cathode and a one-time discharged sulfur cathode. As shown in Fig. 3, the Raman signal of sulfur was detected on the surface of the fresh cathode. As the cell discharged to 1.7 V, the Raman spectrum of the cathode surface shows that the typical sulfur signal (150 cm^{-1} and 220 cm^{-1}) disappeared. Instead a broad peak covering the signal area of polysulfide and sulfide emerged. In contrast, the Raman spectrum of the dense layer formed on the cathode after 50 cycles shows all sulfur related species signals, which is dramatically different from that of the fresh cathode and the one-time discharged cathode. This demonstrates that the dense layer is composed of inactive sulfur and lithium sulfide that accumulated at the separator–cathode interface during cycling.

To fully utilize the polysulfides accommodated in the separators, we propose that a conductive layer with large surface area needs to be in the place at the interface of the separator and the cathode (Fig. 4a). The conductive layer on the surface of the separator was prepared by a facile slurry coating of carbon nanoparticles (Super P, ~30 nm in diameter) with a polyvinylidene fluoride (PVDF) binder (weight ratio 9 : 1). As shown in Fig. 4b and c, the surface of the separator turns from white to black after the slurry coating. The scanning electron microscopy (SEM) image of the pristine separator (Fig. 4d) shows the nanopores (~100 nm in diameter) on the surface of the separator. After the slurry coating, a dense layer of carbon nanoparticles formed on the surface of the separator and covered the nanopores (Fig. 4e). The thickness of the carbon nanoparticle layer coated on the separator was ~1 μm and the mass loading was ~0.5 mg cm^{-2}. We found that this conducting layer does not cause shorting through the 25 μm thick battery separator.

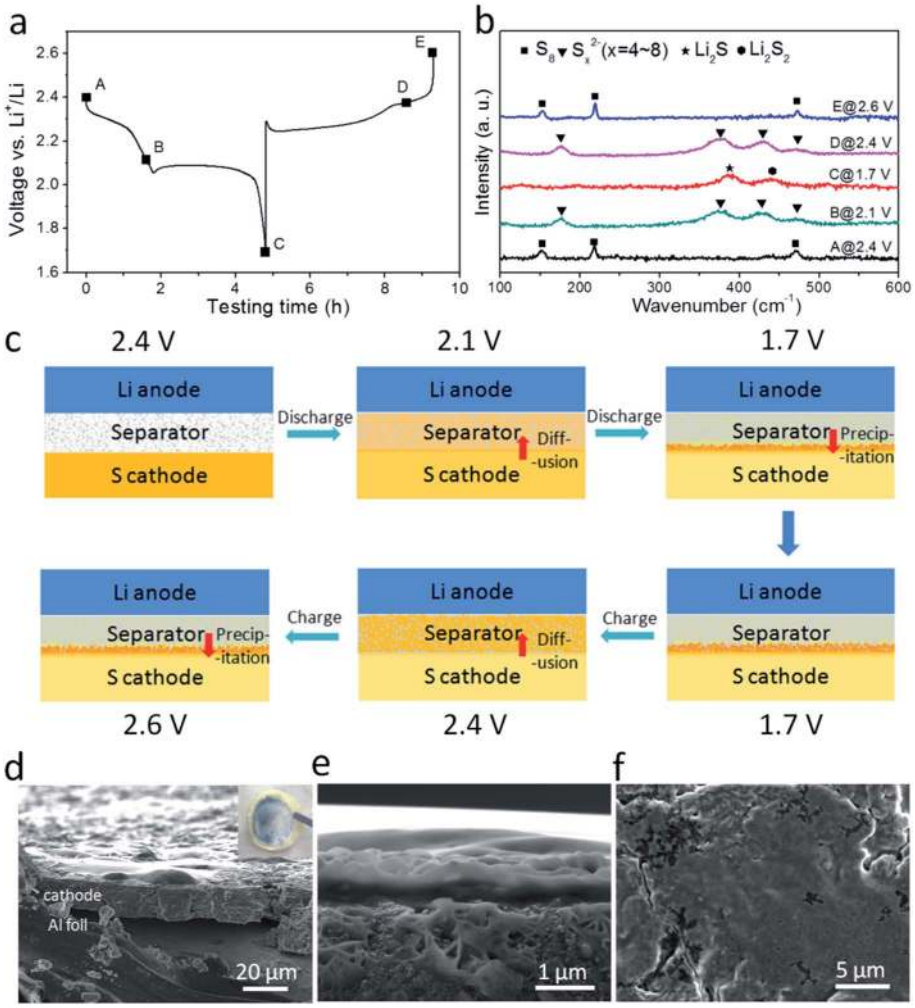

Fig. 2 Polysulfide distribution in the Li–S cell and inactive S related species on the surface of the cathode. (a) Discharge/charge voltage profile of the Li–S cell and typical five voltage points for Raman characterization. (b) Corresponding typical Raman spectra of the cathode at five different discharge/charge voltages. (c) Schematic illustration of sulfur species diffusion, trapping in the separator, and precipitation on the surface of the cathode during charge/discharge processes. (d) Cross sectional SEM image of a normal cathode after 50 cycles. The inset is a photo of the separator attached to the cathode. (e) Magnified cross-sectional SEM image of the cathode after 50 cycles. (f) SEM image of the normal cathode surface after 50 cycles.

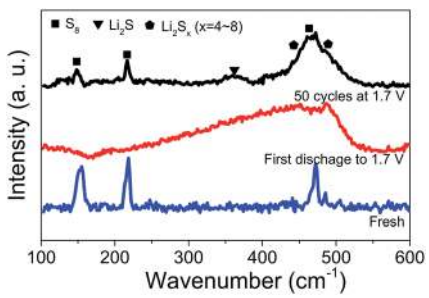

Fig. 3 Raman spectra of the top surface of the fresh sulfur cathode (blue line), the top surface of the sulfur cathode after one-time discharge to 1.7 V (red line), and the top surface of the sulfur cathode after 50 charge/discharge cycles then kept at discharge status at 1.7 V (black line).

The modified separator was coupled with a lithium metal anode and a sulfur cathode to test its effect on Li–S battery performance. The cathode was made of precipitated sulfur powder, Super P, and PVDF, in which the sulfur mass loading was 1.5–2 mg cm^{-2}. To compare the modified separator with the pristine separator on a fair basis, we account for the mass of conductive coating on the modified separator into the cathode. Counting the mass of the Super P–PVDF coating in the 60 wt% sulfur cathode, the sulfur ratio in the cathode was equivalent to a 50 wt% sulfur cathode. Thus, the electrochemical performance of a 60 wt% sulfur cathode coupled with a modified separator was compared with that of a 50 wt% sulfur cathode with a pristine separator. The first discharge/charge cycle voltage profiles at C/10 (1 C = 1673 mA g^{-1}) of cells with different separators are shown in Fig. 4f. Both cells showed a typical Li–S battery voltage profile with voltage plateaus at 2.3 V and 2.1 V, respectively. The voltage plateau at 2.1 V of the cell with the modified separator

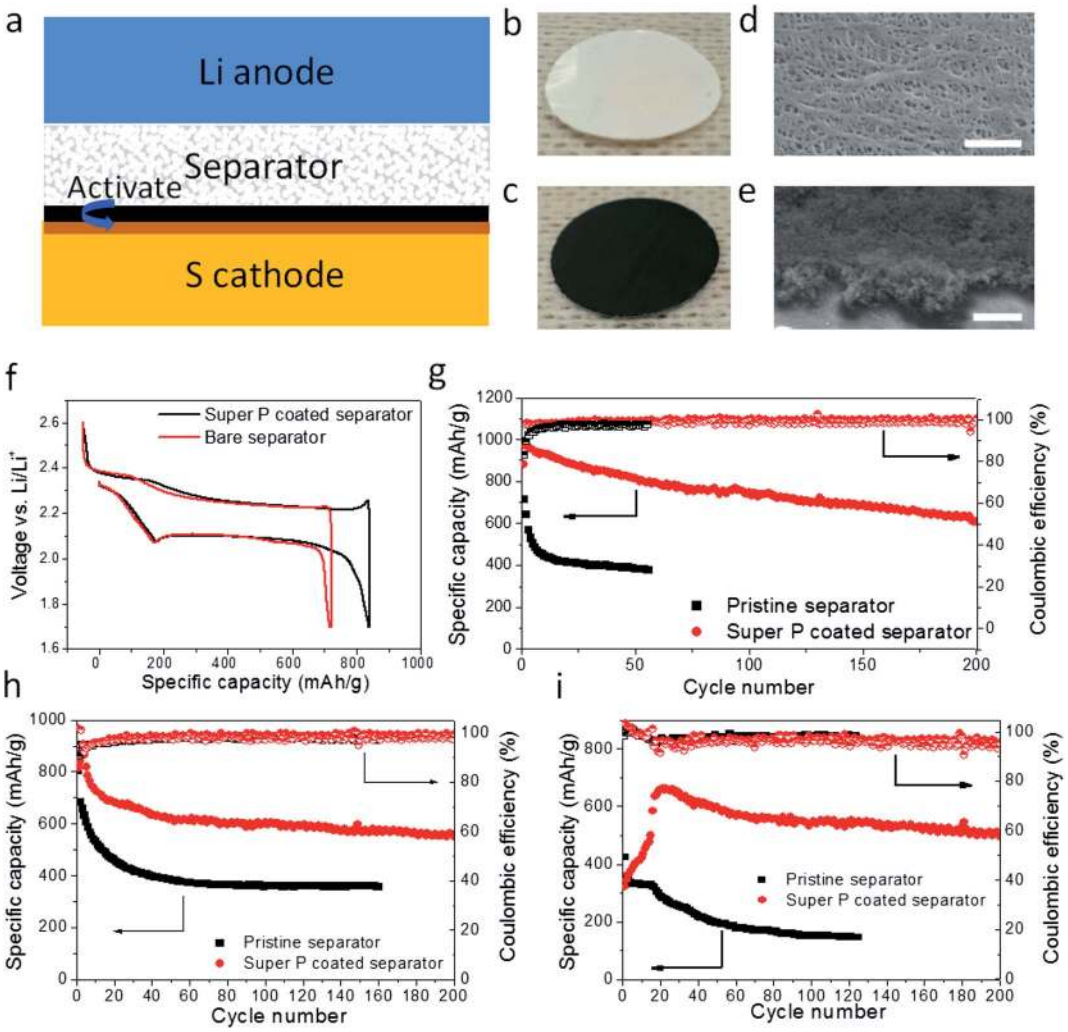

Fig. 4 Separator surface modification and Li–S battery performance comparison. (a) Schematic Li–S battery model with the conductive surface design of the separator. (b) and (c) Photographs, (d) and (e) SEM images of the pristine separator and the Super P coated separator, respectively. Scale bar 2 μm. (f) First discharge/charge voltage profiles of the Li–S battery with different separators. (g) The cycling stability comparison of the Li–S battery (~60 wt% sulfur in the cathode) with different separators at C/10. (h) Cycling stability comparison of the ~70 wt% sulfur cathode–Super P coated separator and the ~60 wt% sulfur cathode–pristine separator, respectively. (i) Cycling stability comparison of the ~80 wt% sulfur cathode–Super P coated separator and the ~70 wt% sulfur cathode–pristine separator, respectively.

was longer than that of the cell with the pristine separator, indicating that the modified separator provided a larger conductive surface for the transformation of polysulfide to solid Li_2S_x ($x = 1, 2$). The initial discharge capacity of the cell with a modified separator can reach up to 836 mA h g^{-1}, which is more than 120 mA h g^{-1} higher than the cell with the pristine separator. The impedance spectra (Fig. S2†) further show that the charge transfer resistance of the battery decreased from 60 Ω to 30 Ω after using the Super P coated separator.[45] The conductive carbon coating on the separator surface increased the conducting surface and thus enhanced the active material utilization in the separator. Fig. 4g shows the cycling stability of the cells with difference separators. Comparing to the rapid capacity decay to ~400 mA h g^{-1} within 50 cycles of the cell with the pristine separator, the capacity of the cell with the Super P coated separator can retain at 610 mA h g^{-1} after 200 cycles with a slow decay rate of 0.1% per cycle. The Li–S cell with the Super P modified separator also shows better rate performance compared to that of the pristine separator (Fig. S3†).

The Super P coated separator also improved the performance of the cathode with higher sulfur ratios. The cycling performance comparisons of the cathodes with 60 wt% and 70 wt% sulfur are shown in Fig. 4h and i, respectively. Both cells with Super P coated separators demonstrated improved specific capacity and cycling stability. The 70 wt% sulfur cathode coupled with the Super P coated separator can retain the specific capacity at ~600 mA h g^{-1} after 200 cycles. Even the cathode with the sulfur content as high as 80 wt% can cycle well by pairing it with the Super P coated separator. After 200 cycles the specific capacity of the 80 wt% sulfur cathode can still reach around 500 mA h g^{-1}. For a fair comparison, the 70 wt% sulfur cathode with a pristine separator only retained the specific

capacity as low as 200 mA h g^{-1} after 50 cycles. Overall, the specific capacity of S materials goes down with the increase of S weight percentage in the electrode, which is an indication that the conducting surface might be a limiting factor for S-related species deposition. The cells with the modified separator and the pristine separator show similar average Coulombic efficiency above 95% with a $LiNO_3$ additive used in the electrolyte.[25,47] To separate the effects of $LiNO_3$ and lithium polysulfide transport in the separator on the Coulombic efficiency, a control cell using the electrolyte without $LiNO_3$ was tested. The first charge/discharge voltage profiles of the cells using the electrolyte with $LiNO_3$ and without $LiNO_3$ are shown in Fig. 5a, respectively. Obviously, the cell using the electrolyte without $LiNO_3$ delivered lower discharge capacity and higher charge capacity indicating the lower Coulombic efficiency. This is consistent with our proposed mechanism of the activation role of the carbon coating on the separator. The conductive carbon coating on the separator can not effectively block the diffusion of polysulfides to the anode due to its relatively low thickness (~2 μm). Our design on the separator is to provide a conductive surface for the redox of polysulfides accommodated in the separator to prevent the formation of an inactive S-related species layer at the interface of the separator and the cathode. The cycling testing (Fig. 5b) shows that the Super P coating on the separator still helps improve the cycle stability of the battery, independently of adding $LiNO_3$ into the electrolyte or not.

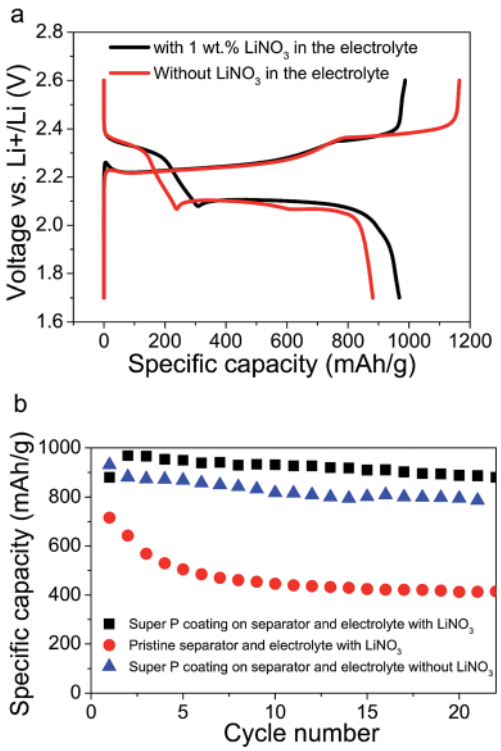

Fig. 5 (a) The first charge/discharge voltage profiles of the Li–S batteries using the electrolyte with 1 wt% $LiNO_3$ and without $LiNO_3$, respectively. ~60 wt% sulfur cathode–Super P coated separator, C/10. (b) The cycling stability comparison of the Li–S battery (~60 wt% sulfur in the cathode) with different separators and electrolytes at C/10.

To confirm the role of the conductive Super P coating on the separator for improving polysulfide utilization, the Li–S coin cell was disassembled after 50 cycles with the discharge potential held at 1.7 V and the separator–cathode interface was characterized by SEM. The inset in Fig. 6a shows the Super P coated separator after 50 cycles. The relatively light color of the Super P coated separator indicates that most of the polysulfides in the separator diffused back and precipitated on the conductive surface. Fig. 6a shows that the Super P modified separator was tightly bound to the cathode indicating a strong bonding interaction between the modified separator and the cathode. At the interface of the Super P modified separator and the cathode, the small bridge-like structures were observed rather than the dense layer appeared on the surface of cathode with the normal separator (Fig. 6b). The top surface SEM images of cathodes (Fig. 6c) further show that the cathode still maintained the porous structure without any dense layer. These results indicate that the Super P coating on the separator offers a large conducting surface area for S-species deposition. Meanwhile, the maintained porous structure of cathode would facilitate the polysulfide diffusion deep inside the cathode, and thus increasing the utilization of polysulfides accommodated in the separator. To show the unique advantage of the Super P coating on the separator, we coated the carbon nanoparticles directly on the sulfur cathode surface and tested their cycling performance. The result is shown in Fig. S4a.† The carbon coating on the cathode cannot retard the fast capacity decay in the first 50 cycles as the coating on the separator does. Similar to the pristine cathode, a dense inactive S-related species layer formed on the surface of the carbon coating on the cathode after 50 cycles as well (Fig. S4b†).

Other nanoparticles were also coated on the separators to further study the influence of coating material properties (*e.g.* surface area, conductivity, and interaction with polysulfides) on the battery performance. Ketjenblack (~30 nm in diameter) and multiwall carbon nanotubes (MCNTs, ~80 nm in diameter) were tested due to their high conductivity and surface area. As shown in Fig. S5a and b†, the Ketjenblack and MCNTs were coated on separators forming a dense layer in both cases. The battery performance with these carbon coated separators is summarized in Fig. 7a. Compared to Super P, the Ketjenblack and MCNT coating on the separator can improve the initial specific capacity of the 60 wt% sulfur cathode from 700 mA h g^{-1} to 1100 mA h g^{-1} at C/5. The specific capacity of the cell with the Ketjenblack or MCNT coated separator can be retained at 760 mA h g^{-1} after 150 cycles. The better performance of Ketjenblack and MCNT coating compared to Super P coating is attributed to their higher electronic conductivities (Table S1†), which would increase the utilization of polysulfides in the separator.

Metal oxide nanoparticles were also tested since they offer stronger binding of Li_xS species.[48,49] The morphologies of TiO_2 nanoparticles–Super P and Al_2O_3 nanoparticles–Super P coatings on the separator are shown in Fig. S5c and d,† respectively, which are similar to that of the Super P coating on the separator. However, adding the metal oxide nanoparticles into the Super P carbon coating layer deteriorates the Li–S battery performance.

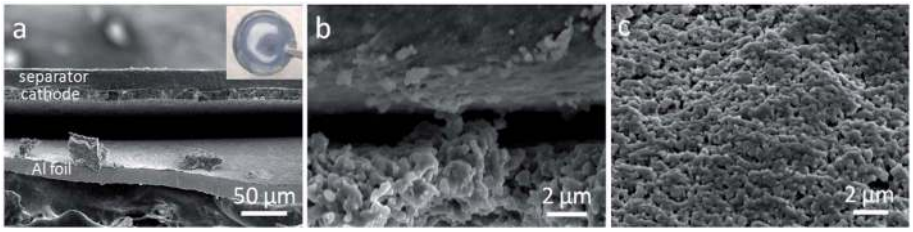

Fig. 6 SEM images of the cathode–Super P coated separator interface and the cathode surface. (a) Cross sectional SEM image of the Super P coated separator–cathode (60 wt%)–Al substrate after 50 cycles. The inset is the photo of the Super P coated separator after 50 cycles. (b) Magnified cross sectional SEM image of the Super P coated separator–cathode (60 wt% sulfur). (c) SEM image of the cathode (60 wt% sulfur, coupled with Super P coated separator) surface.

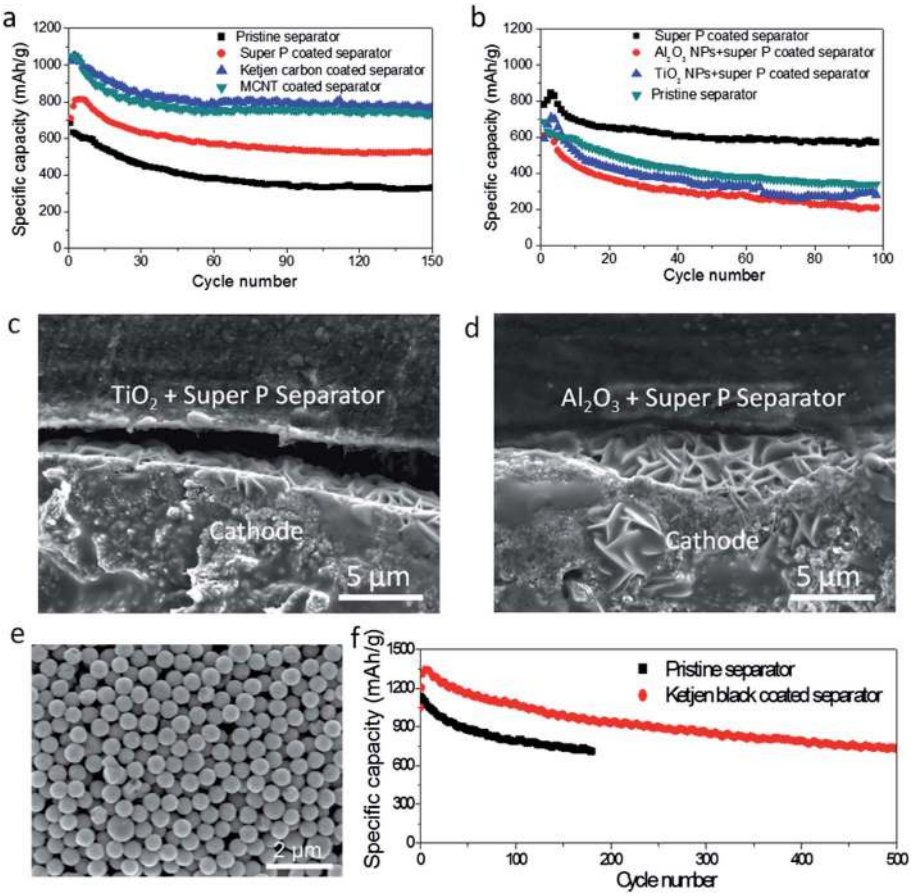

Fig. 7 Li–S cells performance comparison with different materials coating on separators. (a) Cycling stability comparison of Li–S cells with different carbon nanomaterial coatings. Cycle rate, C/5. (b) Cycling stability comparison of Li–S cells with different metal oxides nanomaterial coatings. (c) and (e) Cross sectional SEM images of the TiO_2–Super P coated separator–cathode interface and the Al_2O_3–Super P coated separator–cathode interface. (e) SEM image of as-synthesized polypyrrole coated sulfur nanoparticles showing that the diameter of these particles is ~800 nm. (f) Cycling performance of the Li–S cell by using a Ketjenblack carbon coated separator and a polypyrrole coated sulfur nanoparticle cathode. Cycle rate, C/2.

As shown in Fig. 7b, the specific capacity of the cell with the TiO_2–Super P coated separator or the Al_2O_3–Super P coated separator decayed from 700 mA h g^{-1} to 300 mA h g^{-1} after 50 cycles at C/5, which is even faster than the cell with a pristine separator. To explore the mechanism for fast decay of the cell with using metal oxides in the coating layer, the separator–cathode interface of these cells were characterized by SEM after 50 cycles at the discharge status. As Fig. 7c and d show, a layer of dense film was formed at the interface of the separator and the cathode. This dense film indicates that there is not adequate conducting surface area for S-species deposition since TiO_2 and Al_2O_3 particles have low conductivity. Based on these cases, the requirements for a good coating on the separator surface include high conductivity and high surface area. To further

improve the Li–S battery performance, the Ketjenblack carbon coated separator was combined with polymer (polypyrrole)-coated monodispered sulfur nanoparticles with ~800 nm diameter (Fig. 7e) synthesized in our lab. As shown in Fig. 7f, the fabricated cell delivered a specific capacity as high as 1350 mA h g^{-1} at C/2, which is 230 mA h g^{-1} higher than the cell with the pristine separator.[43] After 500 cycles, the cell still retained 740 mA h g^{-1} of its capacity, showing the decay rate as low as 0.09% per cycle.

Conclusion

In summary, a rational design of coating a conductive layer onto the separator to improve Li–S battery performance was proposed based on the investigation of the polysulfides accommodated in the separator. The large surface area of the conducting coating increased the utilization of the polysulfides accommodated in the separator. We showed that the Li–S battery performance was significantly improved with this conducting layer on the separators. This separator surface modification method opens new avenues to fabricate high performance Li–S batteries.

Acknowledgements

This work was supported by the Assistant Secretary for Energy Efficiency and Renewable Energy, Office of Vehicle Technologies of the U.S. Department of Energy.

References

1 J. M. Tarascon and M. Armand, *Nature*, 2001, **414**, 359–367.
2 M. Armand and J. M. Tarascon, *Nature*, 2008, **451**, 652–657.
3 W. Tang, Y. Zhu, Y. Hou, L. Liu, Y. Wu, K. P. Loh, H. Zhang and K. Zhu, *Energy Environ. Sci.*, 2013, **6**, 2093–2104.
4 H. Gwon, J. Hong, H. Kim, D.-H. Seo, S. Jeon and K. Kang, *Energy Environ. Sci.*, 2014, **7**, 538–551.
5 V. Palomares, P. Serras, I. Villaluenga, K. B. Hueso, J. Carretero-Gonzalez and T. Rojo, *Energy Environ. Sci.*, 2012, **5**, 5884–5901.
6 R. Tripathi, S. M. Wood, M. S. Islam and L. F. Nazar, *Energy Environ. Sci.*, 2013, **6**, 2257–2264.
7 S. Evers and L. F. Nazar, *Acc. Chem. Res.*, 2012, **46**, 1135–1143.
8 A. Manthiram, Y. Fu and Y.-S. Su, *Acc. Chem. Res.*, 2012, **46**, 1125–1134.
9 Y. Yang, G. Zheng and Y. Cui, *Chem. Soc. Rev.*, 2013, **42**, 3018–3032.
10 P. G. Bruce, S. A. Freunberger, L. J. Hardwick and J.-M. Tarascon, *Nat. Mater.*, 2012, **11**, 19–29.
11 C. Barchasz, J.-C. Leprêtre, F. Alloin and S. Patoux, *J. Power Sources*, 2012, **199**, 322–330.
12 S.-E. Cheon, K.-S. Ko, J.-H. Cho, S.-W. Kim, E.-Y. Chin and H.-T. Kim, *J. Electrochem. Soc.*, 2003, **150**, A796–A799.
13 S.-E. Cheon, K.-S. Ko, J.-H. Cho, S.-W. Kim, E.-Y. Chin and H.-T. Kim, *J. Electrochem. Soc.*, 2003, **150**, A800–A805.
14 Y. V. Mikhaylik and J. R. Akridge, *J. Electrochem. Soc.*, 2004, **151**, A1969–A1976.
15 J. Shim, K. A. Striebel and E. J. Cairns, *J. Electrochem. Soc.*, 2002, **149**, A1321–A1325.
16 H. Yamin and E. Peled, *J. Power Sources*, 1983, **9**, 281–287.
17 M. Hagen, P. Schiffels, M. Hammer, S. Dörfler, J. Tübke, M. J. Hoffmann, H. Althues and S. Kaskel, *J. Electrochem. Soc.*, 2013, **160**, A1205–A1214.
18 R. Elazari, G. Salitra, Y. Talyosef, J. Grinblat, C. Scordilis-Kelley, A. Xiao, J. Affinito and D. Aurbach, *J. Electrochem. Soc.*, 2010, **157**, A1131–A1138.
19 R. Demir-Cakan, M. Morcrette, Gangulibabu, A. Gueguen, R. Dedryvere and J.-M. Tarascon, *Energy Environ. Sci.*, 2013, **6**, 176–182.
20 Y. Yang, G. Zheng and Y. Cui, *Energy Environ. Sci.*, 2013, **6**, 1552–1558.
21 L. Xiao, Y. Cao, J. Xiao, B. Schwenzer, M. H. Engelhard, L. V. Saraf, Z. Nie, G. J. Exarhos and J. Liu, *Adv. Mater.*, 2012, **24**, 1176–1181.
22 N. Jayaprakash, J. Shen, S. S. Moganty, A. Corona and L. A. Archer, *Angew. Chem., Int. Ed.*, 2011, **50**, 5904–5908.
23 C. Liang, N. J. Dudney and J. Y. Howe, *Chem. Mater.*, 2009, **21**, 4724–4730.
24 J. Guo, Y. Xu and C. Wang, *Nano Lett.*, 2011, **11**, 4288–4294.
25 G. Zheng, Y. Yang, J. J. Cha, S. S. Hong and Y. Cui, *Nano Lett.*, 2011, **11**, 4462–4467.
26 X. Ji, K. T. Lee and L. F. Nazar, *Nat. Mater.*, 2009, **8**, 500–506.
27 Z. Wei Seh, W. Li, J. J. Cha, G. Zheng, Y. Yang, M. T. McDowell, P.-C. Hsu and Y. Cui, *Nat. Commun.*, 2013, **4**, 1331.
28 W. Li, G. Zheng, Y. Yang, Z. W. Seh, N. Liu and Y. Cui, *Proc. Natl. Acad. Sci. U. S. A.*, 2013, **110**, 7148–7153.
29 Y.-S. Su and A. Manthiram, *Chem. Commun.*, 2012, **48**, 8817–8819.
30 Y.-S. Su and A. Manthiram, *Nat. Commun.*, 2012, **3**, 1166.
31 X. Yu, J. Xie, J. Yang and K. Wang, *J. Power Sources*, 2004, **132**, 181–186.
32 J. Wang, J. Yang, J. Xie and N. Xu, *Adv. Mater.*, 2002, **14**, 963–965.
33 J. Hassoun and B. Scrosati, *Angew. Chem., Int. Ed.*, 2010, **49**, 2371–2374.
34 A. Hayashi, T. Ohtomo, F. Mizuno, K. Tadanaga and M. Tatsumisago, *Electrochem. Commun.*, 2003, **5**, 701–705.
35 J. E. Trevey, J. R. Gilsdorf, C. R. Stoldt, S.-H. Lee and P. Liu, *J. Electrochem. Soc.*, 2012, **159**, A1019–A1022.
36 L. Suo, Y.-S. Hu, H. Li, M. Armand and L. Chen, *Nat. Commun.*, 2013, **4**, 1481.
37 G. Zhou, S. Pei, L. Li, D.-W. Wang, S. Wang, K. Huang, L.-C. Yin, F. Li and H.-M. Cheng, *Adv. Mater.*, 2014, **26**, 625–631.
38 J.-Q. Huang, Q. Zhang, H.-J. Peng, X.-Y. Liu, W.-Z. Qian and F. Wei, *Energy Environ. Sci.*, 2014, **7**, 347–353.
39 Z. Jin, K. Xie, X. Hong, Z. Hu and X. Liu, *J. Power Sources*, 2012, **218**, 163–167.
40 S. S. Zhang, *J. Power Sources*, 2007, **164**, 351–364.
41 N. Imachi, H. Nakamura, S. Fujitani and J. Yamaki, *J. Electrochem. Soc.*, 2012, **159**, A269–A272.
42 J. Y. Kim and D. Y. Lim, *Energies*, 2010, **3**, 866–885.

43 W. Li, Q. Zhang, G. Zheng, Z. W. Seh, H. Yao and Y. Cui, *Nano Lett.*, 2013, **13**, 5534–5540.
44 J.-T. Yeon, J.-Y. Jang, J.-G. Han, J. Cho, K. T. Lee and N.-S. Choi, *J. Electrochem. Soc.*, 2012, **159**, A1308–A1314.
45 N. A. Cañas, K. Hirose, B. Pascucci, N. Wagner, K. A. Friedrich and R. Hiesgen, *Electrochim. Acta*, 2013, **97**, 42–51.
46 Z. Deng, Z. Zhang, Y. Lai, J. Liu, J. Li and Y. Liu, *J. Electrochem. Soc.*, 2013, **160**, A553–A558.
47 D. Aurbach, E. Pollak, R. Elazari, G. Salitra, C. S. Kelley and J. Affinito, *J. Electrochem. Soc.*, 2009, **156**, A694–A702.
48 X. Ji, S. Evers, R. Black and L. F. Nazar, *Nat. Commun.*, 2011, **2**, 325.
49 Y. J. Choi, B. S. Jung, D. J. Lee, J. H. Jeong, K. W. Kim, H. J. Ahn, K. K. Cho and H. B. Gu, *Phys. Scr.*, 2007, **2007**, 62.

